Borrower: MFL

Lending String: *CNO,CLO,CIT,NHM,IQU

Patron: Chaffey, Mark

Journal Title: The Journal of strain analysis for engineering design /

Volume: 25 **Issue:** 2
Month/Year: 1990**Pages:** 75-84

Article Author:

Article Title: Raoof, M.; Effect of hydrostatic pressure on strand behaviour

Imprint: London ; New York ; Published by Mechani

ILL Number: 72001317

Billing: Exempt
Maxcost:$20IFM

Shipping Address:
CSU Moss Landing Marine Labs
Library
8272 Moss Landing Road
Moss Landing, CA 95039

Deliver:
Ariel: 192.190.45.28
Email: library@mlml.calstate.edu
Odyssey:mlml.calstate.illiad.oclc.org

EFFECT OF HYDROSTATIC PRESSURE ON STRAND BEHAVIOUR

M. RAOOF *Civil and Structural Engineering Department, South Bank Polytechnic, London*

High density, supposedly impermeable, polythene sheaths have been offered by cable manufacturers for corrosion protection of large diameter spiral strands used in deep water floating production systems.

Using previously reported orthotropic sheet theory, an insight is given into the effect of high external pressure on various sheathed cable characteristics, which include:

(1) axial stiffness and hysteresis;
(2) torsional stiffness and hysteresis;
(3) free bending fatigue behaviour in the vicinity of end terminations.

It is shown that such high pressures can significantly alter the pattern of interwire/interlayer contact forces. Recent published research has clearly demonstrated the central role such interwire contact pressures play as regards cables' fatigue life under various modes of loading. The present theory shows that increases in contact forces in deep water sheathed cable applications lead to significant reductions in cable fatigue life.

Moreover, such high external forces are shown to affect cables' axial and torsional characteristics by suppressing the relative slippage of wires in the strand and increasing frictional forces between them. A higher cable stiffness will then follow. This then leads to significant variations in strands' axial and/or torsional hysteresis which may have a considerable bearing on the overall dynamics of, for example, a guyed tower platform using sheathed strands.

The significant influence of high external pressures on various cable characteristics have been demonstrated by numerical examples on a realistic 39 mm outside diameter (OD) multi-layered structural strand. Results are also presented for the case of zero external pressure relevant to *unsealed* mooring cables in deep water applications, in which case the absence of the sheath will permit water migration inside the strand and the cable behaviour is independent of the level of water depth.

1 INTRODUCTION

The theoretical analysis of a practical multi-layered strand has been reported elsewhere **(1)–(5)**†. Axial, torsional, and free bending load cases have all been addressed. These analyses have led to predictions of wire strain, interwire forces and slippage, strand stiffness, and hysteresis. The match between carefully conducted large-scale experimental work and theory has been very encouraging **(6) (7)**.

Essentially, the other studies paid too little attention to the effects of interwire contacts on overall strand behaviour, and rather too much attention to small (six or seven wire) strands. Accordingly, a substantial effort has been put into assessing contact forces and the associated relative displacements between wires, taking full account of frictional effects in large (multi-layered) strands.

The other novelty in the study is the treatment of the layers in a strand as a series of pre-stressed orthotropic sheets (one per layer), Fig. 1. Thus, each layer of wires, although discontinuous, has its elastic properties 'averaged' in a way familiar in the analysis of stiffened plating for bridge decks and ship structures. Results from contact stress theory are used to determine the properties of the orthotropic sheets, whose principal axes run parallel and perpendicular to the individual wire axes. The chief advantage of this approach is that its accuracy improves as the number of wires in a given layer increases, i.e., for practical wire sizes, as the size of strand grows. This desirable situation may be contrasted with the decreasing accuracy and increasing complexity as the number of wires increases associated with certain previously available methods of analysis.

Fairly recently, the cable manufacturers have offered high density and supposedly impermeable polythene sheaths for corrosion protection of large diameter cables in very deep water applications. Under such conditions, the clench forces due to the hydrostatic water pressure may become significant compared with the clench forces inside the cable caused by the mean axial load in, say, a guyed tower or communications and power cable applications.

Such external pressures on a sealed multi-layered strand will tend to suppress the relative slippage of wires in the cable by increasing frictional forces between them. A higher cable stiffness will then follow.

Moreover, high hydrostatic levels lead to significant variations in cable axial and/or torsional hysteresis and the pattern of interwire contact forces. The latter can seriously affect the fatigue performance of the cables in, for example, restrained free-bending occurrences in the sea-bed terminations. Under such conditions, interwire fretting has been identified as the main source of fatigue failure **(2)**.

In what follows, the theory will be extended to cater for the effect of hydrostatic pressure on axial and torsional behaviour of spiral strands, with particular attention paid to variations in the interwire/interlayer contact forces. No such results have previously been made available by either theory or experiments.

1.1 Notation

A	Layer area, wire area
A_{ni}	Net steel area in layer i
A_n	Total net steel area of strand cross-section

The MS. of this paper was received at the Institution on 18 May 1989 and accepted for publication on 21 November 1989

† *References are given in the Appendix.*

0309–3247/90/0400–0075 $02.00 + .05

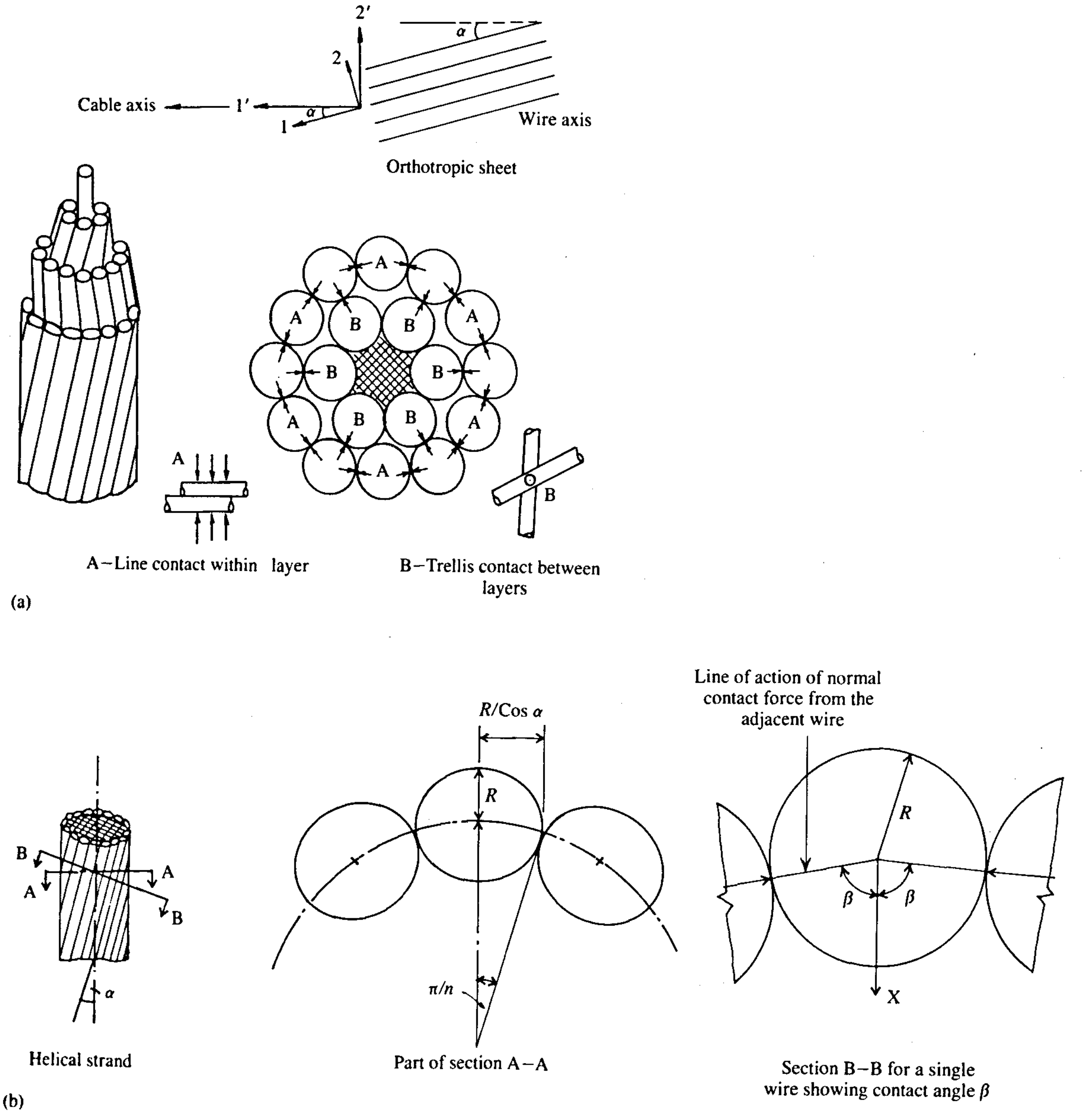

Fig. 1. Wire arrangement in spiral strands: (a) interwine contact forces, (b) geometry

A_{gi}	Gross area of layer i
a	Semi-axis of the ellipse of contact
b	Semi-axis of the ellipse of contact, half-width of the line contact patch
D	Wire diameter
E	Young's modulus
g	Acceleration due to gravity
h	Depth of water
M_i	Internal torque in layer i
n_i	Number of wires in layer i
P_i	Total normal load on a contact patch i
P_{MS}	Circumferential force in a multi-layered strand
P_{RC}	Circumferential force in a single-layer strand
P	Normal load per unit length of line contact patch
p	Normal pressure
R	Cable outer radius
R_i, R'_i	Principal radii of curvature in body i
r_i	Helix radius of layer i
s_i	Strain component (transformation denoted by ′)
S'_{2C}	Total radial strain in a layer with core removed
S'_{2R}	Radial strain due to changes of lay angle
S'_{6T}	Tensorial shear strain
s_{ij}	Compliance (transformation denoted by ′)
T	Axial tension in wire
T_i	Stress component (transformation denoted by ′)
$U, \Delta U$	Maximum stored energy during vibration and loss per cycle
U	Interlayer slippage
X	Radial force per unit length of wire in a given layer
X_H	Magnitude of the hydrostatic force from outside

X_R	Radial clench force transferred from one layer to another
X_{RC}	Radial force in a single layer strand with rigid core
X_{MS}	Radial force in a multi layered strand
x	Spacing between the contact patches along the outer layer
x'	Spacing of contact points on the convex side of wires
α, α'	Lay angle before and after deformation
α', β'	Constants in the Hertz problem
Δ	Tangential displacement at which gross sliding begins
δ	Relative tangential displacement between the centre lines of two adjacent wires
δ_n	Normal approach of distant points in the Hertz problem
ε	Axial strain
ε_c	Cable axial strain
ε_h	Wire axial strain
μ	Coefficient of friction
v	Poisson's ratio
ρ	Water density
σ_x	Direct tensile stress at the trailing edge of contact patch
τ	Shear stress
Φ	Angle between planes with curvatures $1/R_1$ and $1/R_2$ in bodies 1 and 2
ϕ	Applied twist

2 ANALYSIS

2.1 Synopsis of earlier studies

The present paper deals with logical developments of earlier work (1) (5). Each layer of wires in a multi-layered strand is treated as a statically indeterminate orthotropic cylinder with a compliant core. Taking a single layer of wires with a core for a given cable axial strain, S'_1, the core is initially removed and the rigid body motion, S'_{2C}, including contact patch deformations, is calculated. Replacing the core, and enforcing compatibility of radial movement, the deformations in the hoop direction and the line contact forces may then be computed as functions of the net radial strain, S'_2, which is the one used for the orthotropic sheet. Detailed derivations are given in (1), where it is shown that the kinematics of a single layer wire 'continuum' may be analysed using the following equations.

$$S'_{2R} = -(S'_1 - S_1) \tag{1}$$

$$S'_{2C} = (1 + S'_1)\frac{\tan \alpha'}{\tan \alpha} - 1 \tag{2}$$

$$S'_2 = S'_{2C} - S'_{2R} \tag{3}$$

$$d\varepsilon_h = \cos \alpha\{1 + (1 + S'_{2R})^2 \tan^2 \alpha\}^{1/2} - 1 \tag{4}$$

$$S_{6T} = \frac{1}{2(1 + S_2)}\{\tan \alpha(1 + S_1 - d\varepsilon_h) - \tan \alpha'\} \tag{5}$$

$$S_1 = \frac{\cos \alpha}{\cos \alpha'}(1 + S'_1) - 1 \tag{6}$$

$$S_{6T} = \left(\frac{S'_1 - S'_2}{2}\right) \sin (2\alpha') \tag{7}$$

$$S_2 = -\frac{S'_1 - S'_2}{2}\cos (2\alpha') + \frac{S'_1 + S'_2}{2} \tag{8}$$

Where S_1 = the axial wire strain, S_2 = the approach strain normal to S_1 between the centres of wires in line contact, S_{6T} = the associated tensorial shear strain, S'_1 = cable axial strain, S'_2 = the radial contraction of the layer in the cable's normal cross-section due to interwire contact deformations; and $d\varepsilon_h$ = the incremental change in axial wire strain once the core is included where the strain due to the 'rigid body' radial movement in the absence of the rigid core is S'_{2R}. α is the original lay angle and α' is the final lay angle. For a cable axial strain S'_1 equations (1)–(8) may be solved as a set of non-linear simultaneous equations to yield values of S_1, α', S'_{2C}, S'_{2R}, S'_2, and S_2.

The change in distance between centres of wires in line contact, δ_n, is then given by

$$\delta_n = S_2 D \tag{9}$$

where D = the wire diameter.

Substituting δ_n in

$$\delta_n = \frac{4P(1 - v^2)}{\pi E}\left(\frac{1}{3} + \ln \frac{D}{b}\right) \tag{10}$$

with

$$2b = 1.6\left[\frac{PD(1 - v^2)}{E}\right]^{0.5} \tag{11}$$

gives the normal force per unit length of the contact patch whose half-width is b. v is Poisson's ratio of the wire material, and E is Young's modulus. Equations (10) and (11) are results from contact stress theory (8) relating to the contact of two parallel cylinders under normal load, P, per unit length of line contact. In a single layer strand with a rigid core, the interwire line contact force, P_{RC} may thus be calculated by setting $P = P_{RC}$.

2.2 Radial load transfer in a multi-layered strand

Until now, a single layered cylinder with a rigid core has been considered. If α, v, E, and D are specified, it is then possible to determine all the deformations and forces in the membrane for any given cable axial strain S'_1. In particular, it is possible to obtain the line contact force between the individual wires in the layer, P_{RC} and radial body forces X_{RC}, for different strains S'_1, where (1)

$$X_{RC} = \frac{T \sin^2 \alpha}{r} \tag{12}$$

In the above $T = EAS_1$, $A = (\pi D^2)/4$, and r is the helix radius; i.e., the distance between the centre of individual wires in the layer to the centre of the cable.

In a multi-layered strand, part of the radial force exerted on any layer is due to the radial body forces in that layer, and part is due to the clenching effects of the outer layers. These effects grow radially inwards and may be simply described from the outermost layer, layer 1. Further details can be found in (1).

In the absence of externally applied uniform hydrostatic pressure, the relationship between line contact forces, P_{MS}, and radial forces, X_{MS}, in the outer layer of a *multi-layered* strand is identical to that between P_{RC}, and

X_{RC} for that layer. However, with the hydrostatic pressure present, X_{RC} and X_{MS} for layer 1 (and, hence, the corresponding P_{RC} and P_{MS}) are no longer the same, and

$$X_{MS_1} = X_{RC_1} + X_H \tag{13}$$

where X_H corresponds to the magnitude of the hydrostatic force from the outside, per unit length of the wire in the outer layer, i.e.

$$X_H = \frac{2\pi R\rho g h}{n \operatorname{Cos} \alpha_1} \tag{14}$$

where h is the depth of water; R is the cable outer radius; ρ is the water density, g acceleration due to gravity, and n is the number of wires in the outer layer whose lay angle is α_1. From the plots of X_{RC} vs P_{RC} for layer 1 it is then possible to obtain values of P_{MS1} corresponding to X_{MS1} for any given cable axial strain S'_1.

For the other (inner) layers, the additional clench force provided (under a cable axial strain S'_1) by each wire in layer i acting on layer $i + 1$ is given by

$$X_{Ri} = EA_i \frac{S_{1i} \operatorname{Sin}^2 \alpha_i}{r_i} - 2P_{MSi} \operatorname{Cos} \beta_i \tag{15}$$

where subscript i = the ith layer; and $A_i = \pi D^2 i/4$. The angle β (9) locates the lines of action of the line contact force, P_{RC}, Fig. 1(b)

$$\operatorname{Cos} \beta = \frac{1}{\operatorname{Sin}^2 \alpha} \left\{ \sqrt{\left[1 + \frac{\tan^2(\pi/2 - \pi/n)}{\operatorname{Cos}^2 \alpha}\right]} - \sqrt{\left(\tan^2\left(\frac{\pi}{2} - \frac{\pi}{n}\right) \times \left[1 + \frac{1}{\operatorname{Cot}^2 \alpha \operatorname{Cos}^2(\pi/2 - \pi/n) \times \{\operatorname{Cos}^2 \alpha + \tan^2(\pi/2 - \pi/n)\}}\right] + \operatorname{Cos}^4 \alpha\right)} \right\} \tag{16}$$

Each wire in layer $j = i + 1$ thus experiences a total radial force

$$X_{MSj} = EA_j \frac{S_{1j} \operatorname{Sin}^2 \alpha_j}{r_j} + X_{Ri} \cdot \frac{x_i}{x'_j} \tag{17}$$

where

$$\frac{x_i}{x'_j} = \frac{n_i}{n_j} \frac{\operatorname{Cos} \alpha_j}{\operatorname{Cos} \alpha_i} \tag{18}$$

where x_i = the spacing between the contact patches along the concave side of layer i, and x'_j = the spacing of the contact points on the convex side of the wires in the layer j.

Using the previously calculated P_{RC}/X_{RC} data for layer $i + 1$, it is then possible to find the corresponding values for P_{MS} and X_{MS} for layer $i + 1$. The process is then repeated, moving in another layer each time until the whole strand has been analysed.

2.3 Calculation of interwire cross-contact pressures

In a realistic helical strand, the outer wires touch the underlying core at a number of isolated points (contact patches) in a trellis pattern. Figure 2 shows the pattern of contact patches for a cross-laid construction. In the following, Hertzian normal contact theory is used to compute the sizes of the contact areas and the distribution of the normal contact stresses over the individual contact regions.

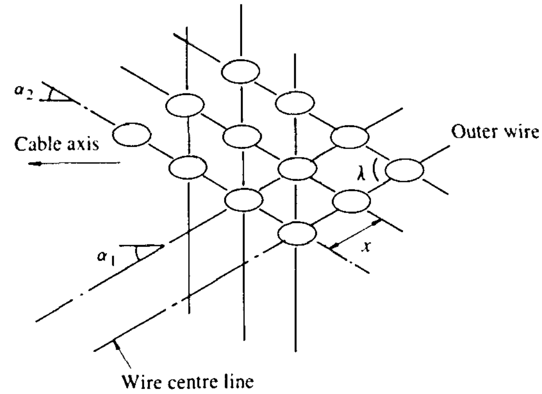

Fig. 2. Interlayer contact patches

The normal load on each of the trellis points of contact, i, between layers i and $j = i + 1$ (where i is the outer layer) is

$$P_i = X_{Ri} \frac{2\pi\rho_i}{n_j} \frac{\operatorname{Cos} \alpha_j}{\operatorname{Sin}(\alpha_i - \alpha_j)} \tag{19}$$

where

$$\rho_i = r_i - \frac{D_i}{2} \tag{20}$$

The semi-axes of the elliptic boundary area

$$a_i = \alpha'(P_i K_D C_E)^{1/3} \tag{21a}$$

$$b_i = \beta'(P_i K_D C_E)^{1/3} \tag{21b}$$

where

$$C_E = 2\left[\frac{1 - \nu^2}{E}\right] \tag{21c}$$

and

$$K_D = \frac{1.5}{1/R_1 + 1/R_2 + 1/R'_1 + 1/R'_2} \tag{21d}$$

$1/R_1$ and $1/R'_1$ are the principal curvatures of body 1, and $1/R_2$ and $1/R'_2$ of body 2. R_1 and R_2 are the minimum radii of curvature, while R'_1 and R'_2 are the maximum radii of curvature. α' and β' are constants whose magnitude is dependent on the parameter θ (8) given by

$$\operatorname{Cos} \theta = \frac{K_D}{1.5} \sqrt{\{(1/R_1 - 1/R'_1)^2 (1/R_2 - 1/R'_2)^2 + 2(1/R_1 - 1/R'_1)(1/R_2 - 1/R'_2) \operatorname{Cos} 2\Phi\}} \tag{22}$$

and Φ is the angle between the plane containing curvature $1/R_1$ in body 1 and the plane containing curvature $1/R_2$ in body 2.

The wires in a strand are of helical shape with curvatures, κ', equal to $\text{Sin}^2\ \alpha/r$. It then follows that

$$R_1 = \frac{D}{2}, \quad R'_1 = \frac{-r}{\text{Sin}^2\ \alpha_1} \tag{23a}$$

$$R_2 = \frac{D}{2}, \quad R'_2 = \frac{r}{\text{Sin}^2\ \alpha_2} \tag{23b}$$

where D is the wire diameter, α the helix angle, with subscripts 1 and 2 denoting the outer and inner layers, respectively. r is the radius of the cylinder on which the contact patches between the two layers lie. It is given with reasonable accuracy by

$$r = r_1 - \frac{D}{2} \tag{24}$$

where r_1 is the helix radius of the outer layer.

Knapp and Chiu (**10**) have recently developed a promising tension fatigue model for helically armoured cables. Their proposed model treats cross-wire Hertz contact stresses as equivalent geometric notches which are then shown to control the cable axial fatigue life. The agreement between their theoretical model and test results has been encouraging. Using the above formulations for the interwire/interlayer contact forces, P, and the size of trellis contact patches, a and b, one can use their technique to analyse the case when the sealed cable is subjected to external uniform hydrostatic pressure. For the present work, it perhaps suffices to mention that the maximum normal pressure on the elliptic interlayer contact patch, p, is given by

$$p = \frac{3}{2}\frac{P}{\pi ab} \tag{25}$$

The subsurface state of stress may be found by contact stress formulas developed by Thomas and Hoerch (**11**) who address the general field of normal contact between non-spherical bodies.

Turning to the question of free bending fatigue close to the termination, experiments (**12**) have shown that the initial wire breaks invariably occur not near the extreme fibre but close to what would be regarded as the neutral axis in a rigid rod. This position can be shown, theoretically and experimentally (**13**), to be the location where the slip between the outer and penultimate layers of wires is largest. Thus interwire or, rather, interlayer fretting is believed to be the most likely cause of wire breakages, and to be much more relevant to a discussion of fatigue life than the maximum wire stress near the extreme fibres. A newly developed alternative may, therefore, be proposed, Fig. 3. Here, the life to 5 per cent outer wire fracture is shown to be controlled by a parameter linking:

(1) the computed maximum tensile stress, σ_x, at the trailing edge of the interlayer contact patch between wires of opposite lay, i.e., at the edge of the so-called 'trellis' contact;
(2) the computed interlayer relative displacement, U, near the neutral axis at a distance equal to the interlayer contact patch spacing along the wire from the assumed ideally fixed end;
(3) the spacing of the trellis contact patches, x.

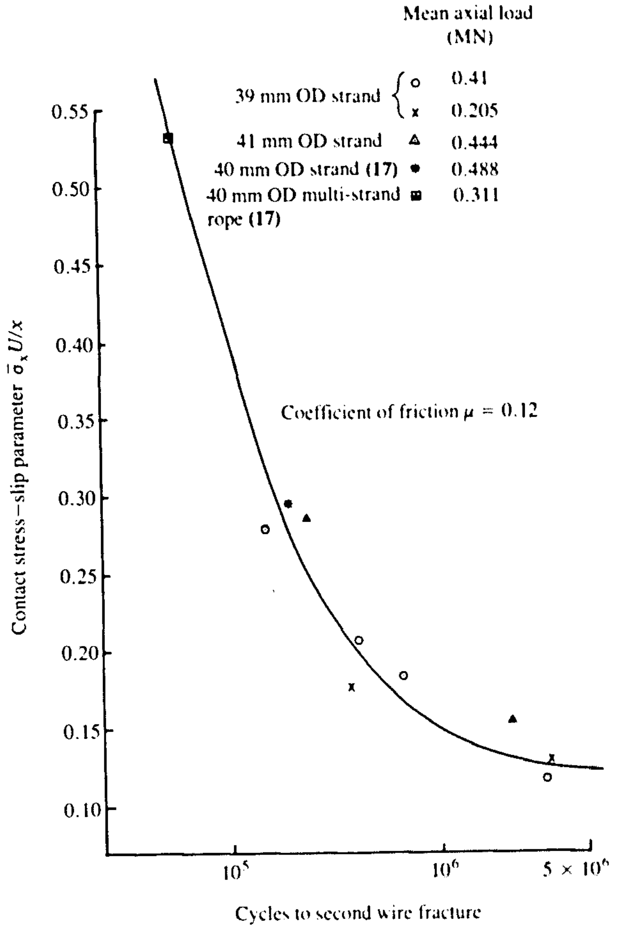

Fig. 3. Free bending fatigue results near termination

Life to 5 per cent of the outer layer wire fracture is a popular but by no means universally accepted indication of incipient overall failure.

The stress σ_x, computed on an elastic basis, has been chosen in view of its likely role in fatigue crack initiation in the individual wires; cracks are commonly found at this location. The value of U near the neutral axis is taken since the slips are largest there.

It is encouraging that the use of this parameter makes it possible to draw a single curve through the experimental data for several realistic multi-layered strands with widely different make-up (i.e., the parameter has predictive value). This may be contrasted with the traditional method of presenting data by plotting the calculated (or measured) maximum extreme fibre wire stresses against fatigue life, where a weak correlation was found in that it was possible to sketch well-separated curves through the data points of each individual strand make up.

A detailed discussion of the method used for obtaining the contact stress–slip parameter is outside the scope of the present paper. For the present purposes it perhaps suffices to mention that the level of external hydrostatic pressure on sealed strands will obviously have a significant effect on the magnitude of the stress, σ_x, and, hence, the magnitude of the contact stress–slip parameter which controls a cable's free bending fatigue life. It then follows that, in deep water guyed tower applications, for example, sea bed termination design should take hydrostatic pressure into account.

2.4 Torsional stiffness

Once the line contact forces between the wires in each layer due to the axial pre-load have been found the layer compliances, s_{ij}, referred to axes 1, 2 of orthotropy parallel and normal to the wire axes, are determined. The compliance parallel to the wire axis, s_{11}, is straightforward, reflecting the ratio between the sheet area and the wire area

$$s_{11} = (4/\pi)E \tag{26}$$

where E is Young's modulus for the wire material, while the coupling term s_{12} is taken as

$$s_{12} = -\nu s_{11} \tag{27}$$

where ν is Poisson's ratio. The normal and shear compliances, s_{22} and s_{66}, between the wires (which are regarded as parallel cylinders in line contact) are obtained from contact stress theory, and are clearly non-linear in the contact force P per unit length. The normal compliance (**1**) is

$$s_{22} = \frac{1}{E}\left(0.11 + 0.59 \ln \frac{ED}{P}\right) \tag{28}$$

where D is the wire diameter, while the shear compliance (**1**) is

$$s_{66} = \frac{s_{22}}{1-\nu}\left(1 - \frac{\delta}{2\Delta}\right)^{-0.5} \tag{29}$$

where δ is the relative tangential displacement between the centre lines of the cylinders, and Δ denotes the tangential displacement from an undisturbed position at which rigid body movement (gross sliding) just starts. The factor of two is needed because, in a cyclic loading, the tangential displacement starts not from an unstressed condition, but from one of slip in an opposite sense. The limiting displacement

$$\Delta = \frac{3}{4}\frac{\mu P}{1-\nu} s_{22} \tag{30}$$

where μ is the coefficient of friction. It is noted that equation (29) holds for $\delta \leqslant 2\Delta$, with s_{66} tending to ∞ at the limit. For larger δ, s_{66}, is taken as ∞.

These tangent compliances referred to the wire axes 1, can be transformed to a set defined in terms of axes 1′, 2′, parallel and normal to the strand axis. If the angle between the two sets of axes (the lay angle of the wires) is α, and $\cos\alpha$, and $\sin\alpha$ are denoted by m and n, respectively, the transformed compliances s'_{ij} are given by (**14**)

$$\begin{aligned}
s'_{11} &= m^4 s_{11} + 2m^2n^2 s_{12} + n^4 s_{22} + m^2n^2 s_{66}\\
s'_{12} &= m^2n^2 s_{11} + (m^4 + n^4)s_{12} + m^2n^2 s_{22}\\
&\quad - m^2n^2 s_{66}\\
s'_{16} &= -2m^3n s_{11} + 2mn(m^2 - n^2)s_{12} + 2mn^3 s_{22}\\
&\quad + mn(m^2 - n^2)s_{66}\\
s'_{22} &= n^4 s_{11} + 2m^2n^2 s_{12} + m^4 s_{22} + m^2n^2 s_{66}\\
s'_{26} &= -2mn^3 s_{11} - 2mn(m^2 - n^2)s_{12} + 2m^3n s_{22}\\
&\quad - mn(m^2 - n^2)s_{66}\\
s'_{66} &= 4m^2n^2 s_{11} - 8m^2n^2 s_{12} + 4m^2n^2 s_{22}\\
&\quad + (m^2 - n^2)^2 s_{66}
\end{aligned} \tag{31}$$

The stress increments T'_i and strain increments S'_i referred to the strand axes are given by

$$\begin{aligned}
S'_1 &= s'_{11}T'_1 + s'_{12}T'_2 + s'_{16}T'_6\\
S'_2 &= s'_{12}T'_1 + s'_{22}T'_2 + s'_{26}T'_6\\
S'_6 &= s'_{16}T'_1 + s'_{26}T'_2 + s'_{66}T'_6
\end{aligned} \tag{32}$$

It is postulated that, in each layer of wires, the changes in the axial and hoop strains on applying any torque increment to the axially pre-loaded strand are zero, i.e., that S'_1 and S'_2 in the first two of equations (32) are zero. Using them to eliminate T'_1 and T'_2, the tangent shear flexibility S'_6/T'_6 can then be obtained from the third equation

$$\frac{S'_6}{T'_6} = s'_{66} + \frac{2s'_{12}s'_{16}s'_{26} - s'_{22}s'^2_{16} - s'_{11}s'^2_{26}}{s'_{11}s'_{22} - s'^2_{12}} \tag{33}$$

If S'_1 and S'_2 are zero, the shear strain increment in the layer, S'_6, is simply

$$S'_6 = r\,\mathrm{d}\phi \tag{34}$$

where $\mathrm{d}\phi$ is the (applied) twist increment per unit length and r is the radius of the wire layer under consideration, and equation (33) can be used to find the corresponding shear stress increment in the layer, T'_6. Integrating both sides of equation (34) the total shear strain is the sum of the increments, or simply $r\phi$. Referred to the wire axes, the total shear strain is thus $r\phi\cos 2\alpha$, and hence the tangential displacement between the wires

$$\delta = Dr\phi\cos 2\alpha \tag{35}$$

where D is again the wire diameter

On the basis of the above development, the following procedure may be applied for any given axial pre-load; i.e., initial line contact force set, to build up the relation between the layer shear stress τ and the twist per unit length ϕ as the sum of a series of twist increments $\mathrm{d}\phi$.

(1) Set $\tau = 0 = \phi$. Calculate s_{11}, s_{12}, s_{22}, Δ, and S'_6 (Equations (26)–(28), (30), and (34)).
(2) Set $\phi = \phi + \mathrm{d}\phi$.
(3) Calculate δ (equations (35)) and hence s_{66} (equation (32)).
(4) Transform the compliances (equations (31)).
(5) Calculate the shear stress increment T'_6 (equation (33)), and the total shear stress by $\tau = \tau + T'_6$.
(6) Return to step (2) as desired.

For any particular twist per unit length, the layer contributes a torque of

$$M_i = \tau A r \tag{36}$$

to the total torque M on the strand.

The layer area

$$A = \pi r D \tag{37}$$

or, in terms of the number of wires, n, in the layer

$$A = \frac{4}{\pi} n \frac{\pi}{4} D^2 \sec\alpha = nD^2 \sec\alpha \tag{38}$$

where the factor $4/\pi$ converts the net wire area to the sheet area, and the factor $\sec\alpha$ allows for the (approximately) oval cross section of the inclined wires as seen in a normal cross section through the strand.

The total torque M is, of course, given by

$$M = \sum_{i=1}^{N} M_i \tag{39}$$

where there are a total of N layers in the strand.

2.5 Axial stiffness

For a strand with its ends fixed against rotation, the elastic constants of the individual sheets along their principal direction of orthotropy may also be transformed to the direction corresponding to the strand axis, equation (32).

The desired axial flexibility of the layer is derived in (5) and is given by the expression

$$\frac{S'_1}{T'_1} = s'_{11} + \frac{T'_2}{T'_1} s'_{12} - \frac{s'_{16}}{s'_{66}} \left(s'_{16} + \frac{T'_2}{T'_1} s'_{26} \right) \tag{40}$$

where it is postulated

$$\frac{T'_2}{T'_1} = \frac{T_2}{T_1} = k, \quad \text{say} \tag{41}$$

k is a function of cable axial strain and for a given S'_1 it is equal to the tangent to the plots of $(P_{MS/O})$ versus $(\pi/4 \cdot ES_1)$; its magnitude is easily obtained by numerical differentiation.

The compliances along the principal directions of orthotropy s_{11}, s_{12}, s_{22}, and s_{66} are given by equations (26)–(29) with transformation given by equation (31). δ in equation (29) is now the line contact displacement per body which, for a given total perturbation (i.e., range) in cable axial strain, S'_1 may be obtained using

$$\delta = 2D \, dS_{6T} = 2DB \, dS'_1 \tag{42}$$

where B = the constant of proportionality between dS_{6T} and dS'_1.

For all practical purposes, it has been found that, for a given mean load and various axial load (strain) ranges, k and s_{22} may be taken as constants. For a given mean strain S'_1 and range dS'_1 the degradation of axial stiffness in each layer (and then for the whole strand) can then be obtained. Axial stiffness is defined on the basis of the net steel area exposed in the strand cross section, A_n, where

$$A_n = \sum A_{ni} = \sum n_i \operatorname{Sec} \alpha_i \frac{\pi D_i^2}{4} \tag{43}$$

The corresponding gross area used for the orthotropic sheet model, A_{gi}, is

$$A_{gi} = \frac{4}{\pi} A_{ni} \tag{44}$$

2.6 Axial and torsional hysteresis

In both cases, the skew-symmetric load displacement diagrams for the loading and subsequent unloading phases of a cyclic movement can be immediately combined to form the hysteresis loop for a given axial preload and cyclic amplitude. The energy dissipation per cycle, $\Delta U/U$ is given by the area enclosed by the loop. An alternative method, based on a treatment of the hysteresis on the individual contacts between the wires, is described elsewhere (15) and yields a check on the calculations.

3 RESULTS AND DISCUSSION

3.1 Interwire normal contact forces and stresses

Figure 4 gives variations of the line contact forces in various layers of the 39 mm OD strand (with construction details given in Table 1 as a function of water depth). The mean axial load in this case is assumed to be zero. Figure 5 shows the way the line contact forces P_{MSi}, in various layers i (outer layer: $i = 1$) vary as a function of cable strain, ε_c, (representing the axial force in the strand). The 39 mm OD strand is assumed to be subjected to 400 m of external water pressure.

At zero cable axial tension, P_{MS} is highest in the outer layer and lowest in the innermost one ($i = 5$). As the cable axial force increases, the internal clench forces grow in magnitude. This in turn increases the level of the line contact forces in the inner layers at a higher rate than that in the outer ones – with high enough tension on the cable, the outer layer will have the lowest P_{MS} among all the other layers in the strand.

Figure 6 shows the variation of two sets (inner and outer) of trellis contact patch maximum normal contact

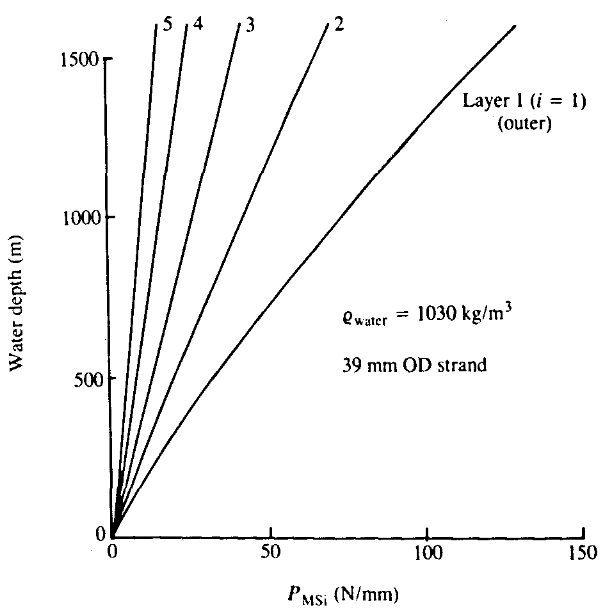

Fig. 4. Variation of line contact forces with water depth

Table 1. Strand make-up for the 39 mm strand

Layer	Number of wires n	Lay direction	Wire diameter D(mm)	Lay angle α(degrees)	Helix radius r(mm)
1	30	RH	3.54	17.74	17.73
2	24	LH	3.54	16.54	14.10
3	18	LH	3.54	15.93	10.57
4	12	RH	3.54	14.90	7.04
5	7	RH	3.54	15.42	4.19
King	1	—	5.05	—	—

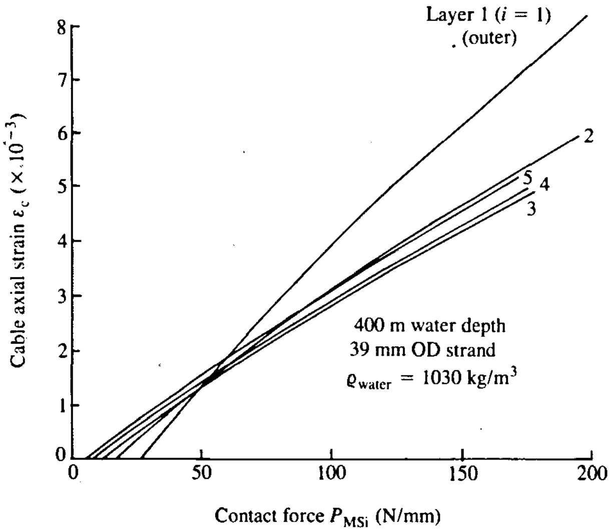

Fig. 5. Variation of line contact forces with axial load for a given water depth

stresses with cable axial tension and the level of externally applied hydrostatic water pressure. The outer set is that between the outer and penultimate cross-laid layers (layers 1 and 2) while the inner set refers to that between layers 3 and 4. Obviously the inner contact patches are subjected to significantly higher levels of stress. A recently developed model for axial fatigue of structural strands in the free field **(10)** provides strong evidence for the central role such interlayer stresses play in determining cables' axial fatigue life. It then follows that, the presence of high externally applied water pressures in, for example, deep water platform applications may have a significant bearing on cables' life in long terms applications. Moreover, individual wire failures are most likely to occur near the sea-bed, with obvious practical inspection problems.

3.2 Torsional stiffness and hysteresis

Figure 7 shows the torque twist relation for the 39 mm OD strand subjected to a mean axial load of 0.42 MN. Even in the absence of hydrostatic pressure, the stiffness of an axially pre-loaded cable subjected to repeated (cyclic) torque perturbations has been shown **(1)** to be a non-linear function of the applied load perturbations. Two clear limiting cases can be established: for small load perturbations superimposed on mean load, no interwire slip occurs, while for large enough disturbances, where fully developed slip takes place, interwire friction becomes negligible compared to force changes in the wires themselves. The theory is capable of predicting these bounds and following the variation between them. From Fig. 7 it is obvious that high external water depths can significantly raise the level of torsional stiffness of the cable. Significant variations in torsional hysteresis with water depth is illustrated in Fig. 8.

The torsional stiffness and hysteresis of spiral strands and electrical conductors are of practical interest in the analysis of certain aero/hydrodynamic problems.

3.3 Axial stiffness and hysteresis

Figure 9 *shows variations of the cable axial stiffness* (secant modulus) as a function of range of axial load to

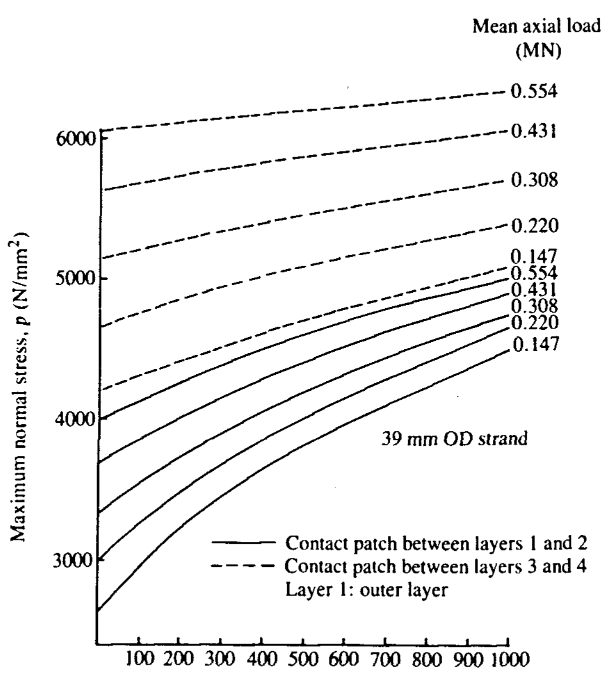

Fig. 6. Variation of maximum normal trellis patch stresses with cable tension and water depth

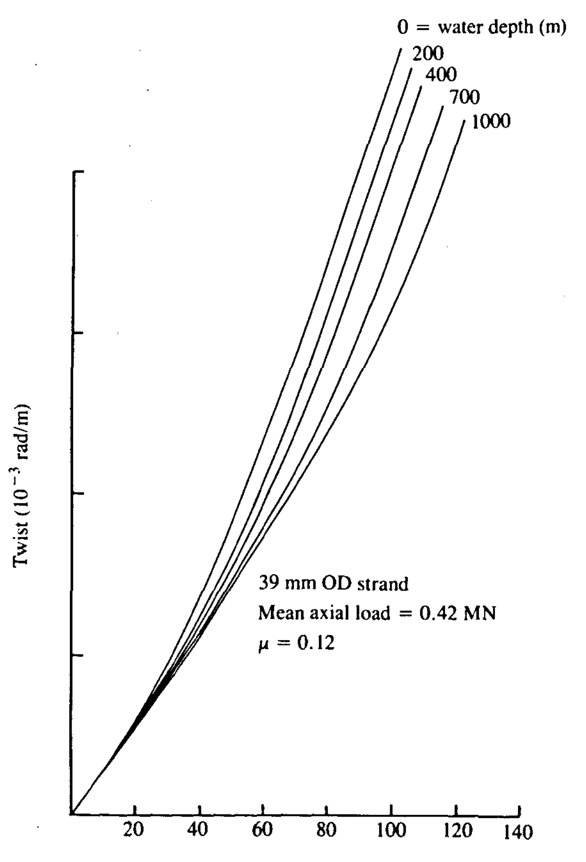

Fig. 7. Cable torque–twist relation for various water depths

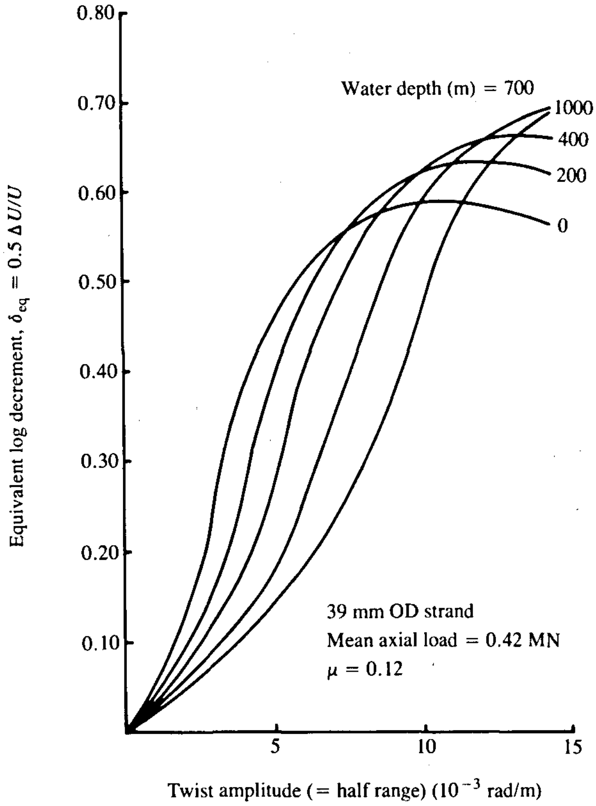

Fig. 8. Variation of strand torsional hysteresis with water depth

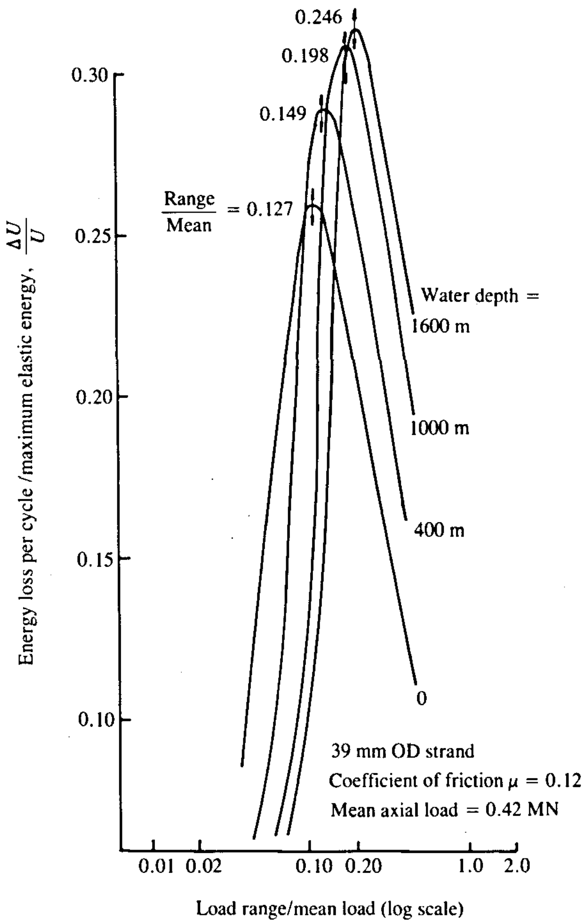

Fig. 10. Variation of strand axial hysteresis with water depth

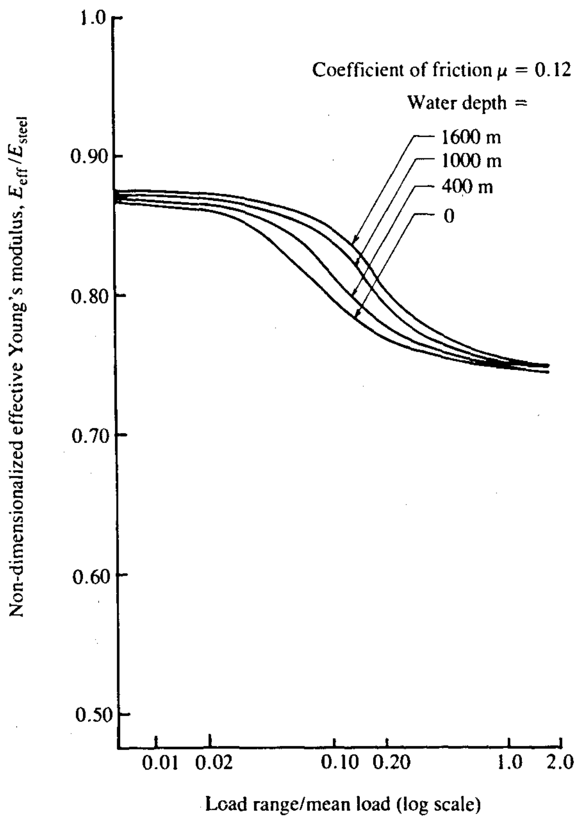

Fig. 9. Variation of strand axial stiffness with water depth

the mean, for various water depths. Similar to the torsional case, two limiting cases of no-slip and full-slip may be identified. The theory is again capable of predicting these bounds and follows variation between them.

Figure 10 shows the way in which the theoretical fully bedded-in cable axial hysteresis may vary with water depth. Increases in the level of external pressure appear to lead to large variations in the magnitude of range to mean axial load at which maximum structural damping takes place. This may have a significant bearing on the overall structural damping characteristics of the moored system.

4 CONCLUSIONS

Some new developments of a model capable of analysing realistic multi-layered strands are presented. An insight is given into the effect of high external hydrostatic pressure on sheathed cable axial/torsional stiffness, hysteresis, and fatigue behaviour.

Using an extended version of previously reported orthotropic theory, it is shown that high external pressures can significantly influence the pattern of interwire/interlayer contact forces in sheathed cables.

The theory shows that, in general, external water pressure on a *sealed* strand used, for example, in a guyed tower platform application, will tend to suppress the slippage of wires in the cable by increasing the frictional forces between them. This will, then, lead to significant variations in the predicted damping behaviour of the cable under both the axial and torsional modes of loading. The two limiting cases of no-slip and full-slip *axial* tangent moduli are, for all practical purposes, independent of the level of external pressure which, nevertheless, does influence the transition between the two limits. Torsional stiffness is found to be very dependent on the level of water depth for all ranges of twist.

Increasing levels of interwire/interlayer contact stresses can have a marked effect on a sealed cable's axial and free bending fatigue life. In particular, results on a realistic 39 mm strand demonstrate a substantial increase in the magnitude of interlayer (trellis) contact patch stresses with increasing levels of external hydrostatic pressure. Such substantial increases in a *sealed* cable's trellis contact patch stresses can lead to significant reductions in cable fatigue life in long term applications. In particular, much attention must be paid to the proper design of sea-bed terminations, taking such effects into account.

ACKNOWLEDGEMENTS

The Author is grateful to Dr R. E. Hobbs of Imperial College, London, for various stimulating discussions.

APPENDIX

REFERENCES

(1) HOBBS, R. E., and RAOOF, M., 'Interwire slippage and fatigue prediction in stranded cables for TLP tethers', *Behaviour of Off-shore Structures*, 1982, edited by C. Chryssostomidis and J. J. Connor (Hemisphere/McGraw Hill, New York) Vol. 2, pp. 77–99.

(2) RAOOF, M. and HOBBS, R. E., 'The behaviour of spiral strand and armored cables close to terminations', *ASME J. Energy Res. Technol.*, 1984, **106**, 349–355.

(3) HOBBS, R. E. and RAOOF, M., 'Hysteresis in bridge strand', *Proc. Instn civ. Engrs*, 1984, **77**, 445–464.

(4) HOBBS, R. E. and RAOOF, M., 'Prediction of the elastic properties of large strands', *Wire Ind.*, 1985, **52**, 39–43.

(5) RAOOF, M. and HOBBS, R. E., 'The analysis of multi-layered structural strands', *J. Engng Mech. Div., ASCE*, 1988, **114**, 1166–1182.

(6) HOBBS, R. E. and RAOOF, M., 'The behaviour of large spiral strands', *Proc. 5th Intl. Symp. Offshore Mechanics and Arctic Engng.*, 1986, edited by J. S. Chung *et al.* (ASME, New York) Vol. 3, pp. 543–549.

(7) RAOOF, M. and HOBBS, R. E., 'Torsion tests on large spiral strands', *J. Strain Analysis*, 1988, **23**, 97–104.

(8) ROARK, R. J. and YOUNG, G. C., *Formulas for stress and strain*, 1975 (McGraw-Hill, New York) International Student Edition.

(9) COSTELLO, G. A. and PHILLIPS, J. W., 'A more exact theory for twisted wire cables', *J. Engng Mech. Div., ASCE*, 1974, **100**, 1096–1099.

(10) KNAPP, R. H. and CHIU, E. Y. C., 'Tension fatigue model for helically armored cables', *ASME J. Energy Res Technol.*, 1988, **110**, 12–18.

(11) THOMAS, H. R. and HOERCH, V. A., 'Stresses due to pressure of one elastic solid upon another', Bulletin No. 212, Engineering Experiment Station, University of Illinois, vol. XXVII, No. 46, Urbana, Il, 1930.

(12) HOBBS, R. E. and GHAVAMI, K., 'The fatigue of structural wire strands', *Int. J. Fatigue*, 1982, **4**, 69–72.

(13) RAOOF, M., 'Free bending of spiral strands', *J. Engng Mech. Div., ASCE*, in press.

(14) HEARMON, R. F. S., *Applied Anisotropic Elasticity*, 1961 (Oxford University Press).

(15) RAOOF, M., *Interwire contact forces and the static, hysteretic, and fatigue properties of multi-layer structural strands*, PhD thesis, University of London, 1983.

(16) STRZEMIECKI, J. and HOBBS, R. E., 'Properties of wire ropes under various fatigue loadings', Imperial College, Civil Engineering Department, CESLIC Report SC6, 1988.